CHEMPHYSCHEM

DOI: 10.1002/cphc.200500303

Asbestos Mineral Analysis by UV Raman and Energy-Dispersive X-ray Spectroscopy

Renate Petry,[a] Remigius Mastalerz,[a] Stefan Zahn,[a] Thomas G. Mayerhöfer,[a] Günther Völksch,[b] Lothar Viereck-Götte,[c] Birgit Kreher-Hartmann,[c] Lothar Holz,[d] Markus Lankers,[d] and Jürgen Popp*[a]

The applicability of a UV micro-Raman setup was assessed for the rapid identification of fibrous asbestos minerals using 257 and 244 nm laser light for excitation. Raman spectra were obtained from six asbestos reference standards belonging to two basic structural groups: the serpentines (chrysotile) and the amphiboles (crocidolite, tremolite, amosite, anthophyllite, and actinolite). The UV Raman spectra reported here for the first time are free from fluorescence, which is especially helpful in assessing the hydroxyl-stretching vibrations. The spectra exhibit sharp bands characteristic of each asbestos species, which can be used for the unambiguous identification of known and unknown asbestos fibres. Evident changes of the relative band intensities sensitively reflect the chemical substitutions that typically occur in asbestos minerals. The elemental composition of the asbestos reference samples was analysed by using a scanning electron microscope equipped with an energy-dispersive X-ray (EDX) spectrometer. The discussion of the experimental results in terms of EDX analysis sheds new light on the structural and vibrational consequences of cation distribution in asbestos minerals.

1. Introduction

Asbestos is a generic name given to a variety of fibrous silicate minerals, which can be divided into two basic mineral groups: the serpentines and the amphiboles. Asbestos minerals (from the Greek "asbestos" = inextinguishable) are the fibrous forms of minerals that occur in bulk or as fibre bundles. They are characterized by unique properties, namely extreme heat resistance, high tensile strength, flexibility, spinnability, and chemical and physical durability. The fibre bundles consist of fibres mostly several centimetres in length; however, they rarely reach metre size. Asbestos fibres have thin needle-like or sometimes flexible structures that may vary widely in diameter within the millimetre to micron range.

Chrysotile (also referred to as "white asbestos") is the only asbestos mineral belonging to the serpentine group, and as the naturally most abundant one it is the most commonly used asbestos fibre in the building industry. Chrysotile is a sheet silicate composed of alternating layers of tetrahedral (T) silica groups (SiO_4) and octahedrally (O) coordinated magnesium groups ($MgO_2(OH)_4$), the local structure of which is comparable to that of Al in kaolinite. However, chrysotile is a trioctahedral sheet silicate with the typical sequence TO-TO, whereas kaolinite consists of TOT groups separated by large interlayer cations (●) according to TOT●TOT●TOT. The fibrous morphology of chrysotile is caused by the slightly warped silicate sheets, which can form hollow fibrils. Structural information on chrysotile has been obtained by X-ray diffraction (XRD) and high-resolution transmission electron microscopy (TEM).[1–5]

The amphibole minerals are double chains of silica tetrahedra with linking cations.[6] The crystal structure of the amphiboles has been evaluated by a variety of methods, such as electron microprobe analysis, TEM and XRD.[7–11] The three amphiboles actinolite, anthophyllite and tremolite make up less than 1% of all naturally occurring asbestos minerals, and their commercial production has been small and sporadic.[12,13] The mineralogical name of crocidolite (also referred to as "blue asbestos") is riebeckite, whereas amosite denotes the fibrous form of the mineral grunerite. Table 1 gives a summary of the pure chemical formulae of the asbestos minerals investigated in this study together with other chemically related minerals that are also structurally related. The most dominant chemical compounds of asbestos minerals are provided in Table 2.

It has already been demonstrated that the combination of data obtained by micro-Raman spectroscopy and scanning electron microscopy/energy-dispersive X-ray (SEM/EDX) analysis provides a powerful tool for the rapid discrimination of asbestos minerals in microscopic quantities.[14,15] Herein, we aim to show that the use of deep-UV micro-Raman spectroscopy

[a] *Dr. R. Petry, R. Mastalerz, S. Zahn, Dr. T. G. Mayerhöfer, Prof. Dr. J. Popp*
Institut für Physikalische Chemie, Universität Jena
Helmholtzweg 4, 07743 Jena (Germany)
Fax: (+49) 3641-948302
E-mail: juergen.popp@uni-jena.de

[b] *Dr. G. Völksch*
Otto-Schott-Institut für Glaschemie, Universität Jena
Fraunhoferstr. 6, 07743 Jena (Germany)

[c] *Prof. Dr. L. Viereck-Götte, Dr. B. Kreher-Hartmann*
Institut für Geowissenschaften, Universität Jena
Burgweg 11, 07749 Jena (Germany)

[d] *Dr. L. Holz, Dr. M. Lankers*
rap.ID Particle Systems GmbH
Ostendstr. 25, 12459 Berlin (Germany)

Table 1. Idealized chemical formulae of asbestos minerals[12] and related silicate minerals (talc) with their localities listed according to commercial exploitation.

Mineral	Chemical formula	Source
Chrysotile	$Mg_3Si_2O_5(OH)_4$	Asbestos mine, Québec, Canada
Crocidolite	$Na_2(Fe^{2+},Mg)_3Fe_2^{3+}Si_8O_{22}(OH)_2$	Oranje River, South Africa
Riebeckite	"	Alintei, Macedonia
Amosite	$(Fe^{2+})_2(Fe^{2+},Mg)_5Si_8O_{22}(OH)_2$	Penge mine, Transvaal, South Africa
Tremolite	$Ca_2Mg_5Si_8O_{22}(OH)_2$	Stemmas, Fichtelgebirge, Germany
Anthophyllite	$Mg_7Si_8O_{22}(OH)_2$	Origätri, Finland
Actinolite	$Ca_2(Fe^{2+},Mg)_5Si_8O_{22}(OH)_2$	Knappenwand, Untersulzbach valley, Austria
Talc	$Mg_3(Si_2O_5)_2(OH)_2$	Greiner, Zillertal, Austria

Table 2. Characteristic elemental composition of asbestos minerals [wt.%][a]

Mineral	SiO_2	Al_2O_3	F_2O_3	FeO	MgO	CaO	Na_2O
Chrysotile	**38–42**	(0–2)	(0–5)	(0–3)	**38–42**	(0–2)	(0–1)
Crocidolite	**49–56**	(0–1)	**13–18**	**3–21**	(0–13)	(0–2)	4–8
Amosite	**49–52**	(0–1)	(0–5)	**35–40**	5–7	(0–2)	(0–1)
Tremolite	**55–60**	(0–3)	(0–5)	(0–5)	**20–25**	**10–15**	(0–2)
Anthophyllite	**53–60**	(0–3)	(0–5)	**3–20**	**17–31**	(0–3)	(0–1)
Actinolite	**51–56**	(0–3)	(0–5)	**5–15**	**12–20**	**10–13**	(0–2)

[a] Major constituents emphasized in bold. Figures in parentheses denote common elemental substitutions found in asbestos minerals.[19]

additionally allows access to the range of OH stretching modes with an unprecedented quality due to the absence of fluorescence. A joint application of UV micro-Raman spectroscopy and SEM/EDX analysis is therefore an ideal combination to assess the nature of fibrous asbestos minerals.

Experimental Section

Samples of fibrous asbestos were kindly provided by the Collection of Mineralogy at the Department of Geology, University of Jena. The localities of the reference samples and idealized chemical formulae are given in Table 1. The chemical composition and the amount of impurities were determined by using an SEM (DSM 940A, Carl Zeiss, Germany) equipped with an EDX analyser (eXL10, Oxford Instruments, UK). Rotating samples were coated with carbon to avoid surface charging in the SEM/EDX system. Operating conditions: 20 kV; $\approx$0.4 nA; 10^{-7}–10^{-6} hPa; 200 s accumulation time, that is, about 500 000 counts/spectrum. Quantitation was done by the Phi–Rho–Z routine using a virtual standard package and a gain calibration (Co) every 3 h.

An intracavity frequency-doubled argon-ion laser (Innova 300, FReD, Coherent) was used to generate the 244- and 257-nm continuous-wave laser lines. The Raman spectra were recorded on a micro-Raman instrument (HR800, Horiba/Jobin Yvon) equipped with a 2400-groove mm^{-1} grating and a cryogenically cooled charge-coupled device (CCD) detector. Due to the $1/\lambda^4$ advantage and potential resonance enhancement, it was possible to keep the recording time comparably low; an integration time of a few minutes was used. The calibration of the spectrometer and the routine check of the laser-beam alignment along the optical pathway were performed daily using Teflon and diamond as reference controls. The maximum power delivered to the sample was typically below $\approx$3 mW when using the 257-nm laser line and less than $\approx$5 mW using the 244-nm laser line for excitation. Incident and 180° back-scattered light was collected by a refractive objective (LMU-40x, Optics for Research) with a working distance of 1 mm, NA of 0.50, and a broadband coating for the deep-UV range with overall transmission of 92%.

2. Results and Discussion

The structure of the amphiboles can be denoted by the general formula $A_{0-1}B_2C_5T_8O_{22}(OH,F)_2$, which allows for separation into several subgroups based on the predominant cations in the B sites, namely the iron–magnesium(–manganese) amphiboles, the calcic amphiboles and the alkali amphiboles.[17] The structural sites A, B, C and T may be occupied as follows: A: Na, K; B: Na, Ca, Mg, Fe^{2+} (also Mn, Li); C: Mg, Fe^{2+}, Al, Fe^{3+} (also Mn, Zn, Cr, Ti and Li); T: Si, Al. Table 3 gives an overview of representative amphibole compositions. Specific names are usually given depending on the substitutions of Fe^{2+} and other divalent ions for Mg in the B sites, and of Fe^{3+} and other trivalent ions for Al in the C sites, expressed by prefixes such as magnesio-, ferro- or alumino-(amphibole). The sodic–calcic group is characterized by the replacement of Ca with Na in the B site (winchite, actinolite), which leads to charge compensation by the substitution of Al for Mg in the C site. Replacement of Ca by Na in the B site may also be coupled with the addition of Na to the A site (e.g. richterite), or with the substitution of Al for Si in the T site, such as in taramite.

Table 4 summarizes the chemical composition of the amphibole minerals investigated in this study by SEM/EDX, thereby following the systematic description and nomenclature as outlined and discussed above (see Table 3). Anthophyllite exhibited structural features very close to the ideal composition, whereas in amosite (the fibrous form of grunerite) substitu-

Table 3. Grouping of amphibole asbestos based on predominant cations in the B sites.

Name	A	B	C	T	Group
Anthophyllite	–	Mg_2	Mg_5	Si_8	
Gedrite	–	Mg_2	Mg_3Al_2	Si_6Al_2	iron–magnesium
Cummingtonite	–	Mg_2	Mg_3Fe_2	Si_8	amphiboles
Grunerite (Amosite)	–	Mg, Fe	Fe_5	Si_8	
Tremolite	–	Ca_2	Mg_5	Si_8	calcic amphiboles
Winchite	–	NaCa	Mg_4Al	Si_8	
Richterite	Na	NaCa	Mg_5	Si_8	sodic–calcic
Taramite	Na	NaCa	Mg_3Al_2	Si_6Al_2	amphiboles
Actinolite	–	$Na_{>1.5}Ca_{<0.5}$	$Mg_2Fe^{2+}{}_3$	$Si_{7.5}Al_{0.5}$	
Glaucophan	–	Na_2	Mg_3Al_2	Si_8	alkali
Riebeckite	–	Na_2	$Fe^{2+}{}_3$, $Fe^{3+}{}_2$	Si_8	amphiboles

Table 4. Results of the energy-dispersive X-ray analysis of amphibole asbestos (stoichiometries result from an average of up to five measurements per sample).

Name	A	B	C	T	Traces
Anthophyllite	–	Mg_2	$Mg_{4.9}Fe_{0.1}$	Si_8	–
Amosite	–	$Mg_{1.6}Fe_{0.12}Mn_{0.28}$	Mg_3Al_2	Si_6Al_2	$\pm Ca_{\leq 0.02}K_{\leq 0.03}$
Tremolite	–	Ca_2	$Mg_{4.9}Fe^{2+}{}_{0.2}$	$Si_{7.8}Al_{0.2}$	–
Mg-riebeckite	$Na_{0.2}K_{0.2}$	$Na_{1.5}Ca_{0.5}$	$Mg_3Fe^{3+}{}_2Al_{0.2}$	Si_8	$\pm Ti_{\leq 0.03}Mn_{\leq 0.1}$
Crocidolite	–	$Na_{1.9}Ca_{0.1}$	$Fe^{2+}{}_{2.2}Mg_{0.8}Fe^{3+}{}_2$	Si_8	$\pm K_{\leq 0.05}$

tions in the B and T sites were detected. The X-ray spectrum of tremolite revealed that Al was substituted for Si and traces of Fe^{2+} replaced Mg in the C site. Within the group of the alkali amphiboles varying amounts of substitutions were observed in the B site, namely in crocidolite ($Na_{1.9}Ca_{0.1}$) and in riebeckite ($Na_{1.5}Ca_{0.5}$). The latter deserved the prefix "magnesio"-, due to the amount of Mg substituted in the C site. As outlined before when discussing the ideal chemical composition of the amphiboles (Table 3), this mineral featured the consequences of charge over-compensation, which clearly was not fully satisfied solely by Na and K entering the A site. The general chemical formula of chrysotile, as a member of the serpentine group, can be denoted by $Mg_3Fe_{<0.1}{}^{3+}[Si_2Al_{<0.1}O_5](OH)_4$. The fibrous sample originating from the asbestos mine in Québec was investigated by SEM/EDX, which revealed traces of Ca, S and Mn ($Mg_3Fe_{0.1}{}^{3+}Ca_{0.1}[Si_2O_5](OH)_4$).

The vibrational assignments of the peaks are given in Table 5. The assignment process is usually complicated in the case of the layer silicates with the exception of the well-separated O–H stretching vibrations, which can be found in the range 3600–3700 cm^{-1} and, to some extent, with the exception of the Si–O stretching vibrations. In the latter case, the most intense band in the region between 900 and 1150 cm^{-1} can usually be attributed to the vibration of nonbridging

Table 5. Wavenumbers[a] [cm^{-1}] and tentative band assignments of the observed UV Raman bands, with excitation at 257 and 244 nm.

Band	Chrysotile $\lambda = 257/244$ nm	Crocidolite $\lambda = 257/244$ nm	Tremolite $\lambda = 257$ nm	Talc $\lambda = 257$ nm	Amosite $\lambda = 244$ nm	Actinolite $\lambda = 244$ nm	Anthophyllite $\lambda = 244$ nm
OH stretch	3696 (vs)/3698 (vs) 3647 (s)/3647 (s)		3675 (vs) 3650 (w, sh)	3676 (vs) 3660 (w)	3630 (m) 3612 (m)	3652 (w) 3309 (w)	3691 (s) 3666 (vs)
Si–O$^-$/Si–O–Si, ν_{as}	1118 (s)/1118 (s)	1102 (ms)/1098 (w) 1026 (vs)/1024 (vs) 960 (s)/959 (w) 860 (ms)/861 (w)	1062 (s) 1031 (m) 933 (m) 752 (w) 740 (w, sh)	1051 (vw) 793 (w) 707 (w)	1018 (s)	1101 (m) 1036 (m)	1052 (s) 1003 (s)
Si–O–Si, ν_s	693 (ms)/693 (vs)	655 (ms)/651 (ms)	676 (vs)	677 (vs)	635 (vs)	666 (vs)	669 (vs)
Si–O–Si, δ/Me–O(H)	530 (m)/531 (m) 389 (w)/388 (vw)	582 (s)/578 (s) 540 (vs)/539 (s)	532 (w) 418 (w) 397 (m) 373 (w) 353 (w) 335 (w)	469 (w) 434 (w)	397 (w)		530 (vs)

[a] Abbreviations: vs, very strong; s, strong; ms, medium strong; m, medium; w, weak; vw, very weak; ν_{as}, antisymmetric stretching vibration; ν_s, symmetric stretching vibration; δ, deformation vibration; sh, shoulder.

oxygen atoms oriented perpendicular to the layer.[17] In some cases, however, this band is not polarized,[18] which is probably a consequence of the curved structure of the fibrous asbestos. Therefore, this band is often attributed to in-plane Si–O vibrations (antisymmetric Si–O–Si stretching vibrations), which occur in the same spectral regions. The symmetric Si–O–Si stretching vibration around 650 cm^{-1} is usually easy to identify due to its strong intensity. Below 600 cm^{-1} Si–O deformation vibrations and M–O(H) stretching vibrations (M = Mg, Fe) generally cannot be discussed separately due to strong mechanical coupling between the vibrations.[17]

2.1. Chrysotile

Micro-Raman experiments were repeatedly performed on each sample (six to eight times) to account for the variability of chemical composition. Representative UV micro-Raman spectra of chrysotile excited at 257 and 244 nm are presented in Figure 1. The spectra are presented as obtained, devoid of fluorescence or background spectrum subtraction, but adjusted for intensity of the most dominant Raman band and shifted vertically for ease of comparison. The spectra contain characteristic Raman bands from the OH^- stretching modes in the higher wavenumber region (> 3600 cm^{-1}) and of the coupled metal–oxygen stretching and Si–O deformation modes in the lower wavenumber region (< 550 cm^{-1}). A number of bands are accompanied by substantial relative intensity changes, as shown in Figure 1 a–c. The positions and assignments of the most dominant Raman bands obtained with 244- and 257-nm excitation are summarized in Table 5. The observed changes in the Raman band intensities reflect the variations of elemental composition that are known to occur in fibrous asbestos minerals (Table 1). However, the ratios of the band intensities may only serve for a semi-quantitative analysis and tentative assignment to particular details of the structure. From inspection of the spectral features observed in Figure 1 a ($\lambda_{exc.}$ = 257 nm) and Figure 1 d ($\lambda_{exc.}$ = 244 nm), it can be concluded that both excitation wavelengths are equally suited to providing information on the unambiguous discrimination between the serpentines and the amphiboles or structurally related silicates (e.g. talc). Kloprogge et al. have commented on the OH stretching region of the serpentines, which show broad bands around 3697 and 3651 cm^{-1} with structures that appear less detailed than in kaolinite.[18] The inner and outer hydroxy groups are said to be indistinguishable from these spectral features in the serpentine minerals.[17] However, Titulaer et al. suggested that the Raman bands in the OH stretching region can be assigned separately to the inner and outer OH groups of the brucite-like layer in chrysotile asbestos.[19] Based on the analogy with kaolinite and from single-crystal Raman microscopic studies on chrysotile, Kloprogge et al. concluded that the higher frequencies in the OH stretching region (≈ 3696 cm^{-1}) can be assigned to the outer OH stretching modes. The inner OH groups, which are located in the lower shared plane of the octahedral sheet,[20–22] are reflected in the distinct Raman band near 3649 cm^{-1}. These assignments were mainly based on the observed Raman-band intensity ratios reported on chrysotile asbestos (close to 3:1) as expected from the crystal structure, which is composed of three external OH groups at the top of the brucite-like sheet and one internal OH group at the bottom of the sheet.[18] This band assignment in the higher wavenumber region allows the characteristic bands of chrysotile and talc to be clearly distinguished. The latter is the 2:1 analogy of chrysotile and shows a single band originating from the OH stretching band near 3677 cm^{-1}, as expected from the centro-symmetric relationship in talc between the hydroxy groups, which are arranged symmetrically on both sides of the octahedral layer. The spectral features obtained by the UV Raman experiments on chrysotile asbestos are thus in very good agreement with earlier reports, and furthermore provide detailed information to distinguish chrysotile from structurally related minerals.[18,19]

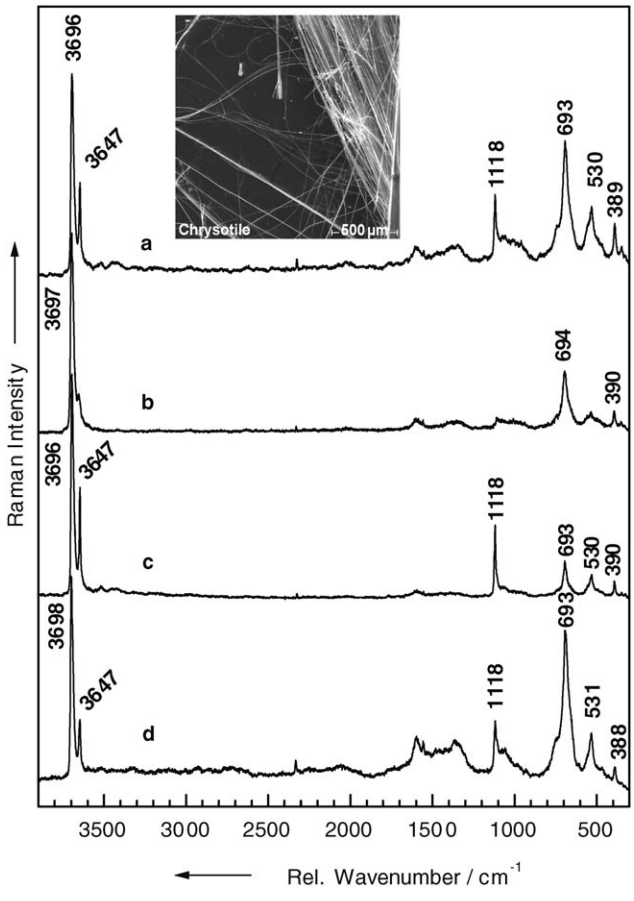

Figure 1. UV micro-Raman spectra of fibrous chrysotile asbestos excited at 257 nm (a–c) and at 244 nm (d). Inset: SEM of chrysotile.

2.2 Crocidolite

The UV Raman spectra of crocidolite obtained with 257- and 244-nm excitation exhibited a high signal-to-noise ratio (Figure 2). The fibrous mineral showed a medium-strong band at 655 cm^{-1}, which lies in the same spectral region as the symmetric Si–O–Si vibration of the other investigated fibrous asbestos minerals, but in contrast to these materials it is not the band with the strongest intensity in the spectrum in accordance with the results from ref. [21]. The strong bands around

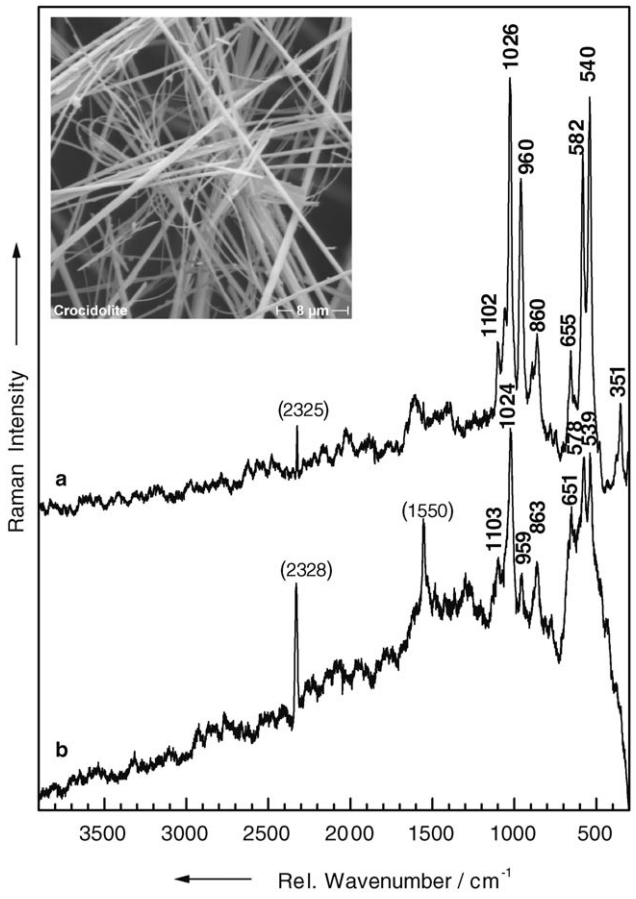

Figure 2. Characteristic UV Raman bands of crocidolite obtained by excitation at 257 nm (a) and at 244 nm (b). Inset: SEM of fibrous crocidolite.

580 and 540 cm^{-1} are often assigned to the Si–O–Si stretching vibrations,[21] but due to their comparably low wavenumbers it is likely that they are not mere stretching vibrations, or should be classified as deformation vibrations.[17] Their band positions are in good agreement with earlier studies using 632.8 nm for excitation.[6,12,15] Interestingly, none of the expected OH stretching modes in the higher wavenumber region could be excited with the 257- or 244-nm laser line. Inspection of the SEM/EDX data of crocidolite revealed that the mineral did not match the ideal chemical composition (see Table 4). In fact, the mineral exhibited a variety of substitutions, for example, Na was partially replaced by Ca in the B site, and Na and K were assigned to be present in the A site. It is known that the substitution of Na for Ca in the B site can be coupled with Na entering the A site.[24] We therefore assume that Na entering the A site leads to a massive suppression of the characteristic OH stretching modes, which usually appear as very strong bands in the higher wavenumber region of the Raman spectrum. Most of the recorded spectra in this study were accompanied by sharp bands at 1550 cm^{-1} (oxygen) and near 2327 cm^{-1} (nitrogen), which originated exclusively from Raman scattering of the ambient air in the laboratory. These bands appeared to be particularly dominant in the weak Raman scattering samples, and showed spectra with low signal-to-noise ratios (e.g. Figure 4b).

2.3 Tremolite

The UV Raman spectra of tremolite (Figure 3) are dominated by a number of very sharp, well-defined bands, such as the characteristic silicon-bridging Si–O–Si symmetric stretching

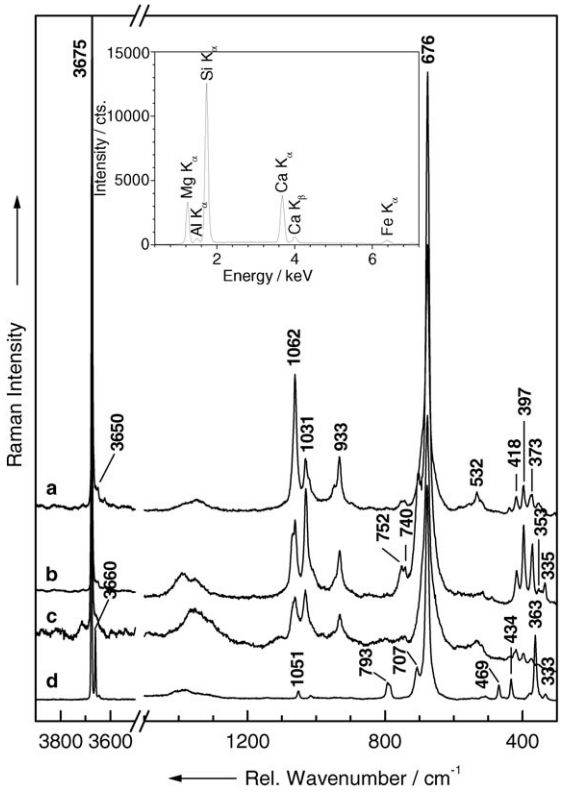

Figure 3. Comparison of UV Raman spectra of tremolite asbestos excited at 257 nm (a, b) and at 244 nm (c). The spectrum of talc (d), recorded at 257 nm excitation, can be differentiated from the asbestos spectrum by several distinct bands in the lower wavenumber region. Inset: energy-dispersive X-ray spectrum of tremolite.

modes of the pyroxene chain at 676 cm^{-1} and from the OH^- stretching modes at 3675 cm^{-1}. The region between 900 and 1100 cm^{-1} exhibits nonbridging Si–O^- stretching modes as well as Si–O–Si bridging modes of the silicate network. The observed UV Raman bands are in good agreement with earlier reports.[6,12,15,23] Our results are also highly consistent with the Raman microprobe spectra obtained from individual microcrystals, fibrous tremolite and other amphiboles reported by Blaha and Rosasco.[25] All asbestos minerals have silicate strips in common, which are formed by cross-linked pyroxene chains to give sheets. In the chain silicates (amphibole group), only two chains are coupled in this fashion, whereas the sheet silicates (serpentine group) are characterized by cross-linked pyroxene chains to form sheets.[16,26] The characteristics of the Raman spectra provide information to establish the major structural unit and its coordination in the lattice. The amphiboles are composed of brucite-like strips that are sandwiched between opposed silicate strips, whereas in talc the structural features are quite similar to those of tremolite due to a brucite sheet

between the silicate sheets. The brucite strip consists of octahedral coordinated cations, which are responsible for the metal–oxygen vibrational modes of the Mg ions in tremolite and talc that arise in the spectral region below 600 cm^{-1}. This region is of particular interest for the unambiguous differentiation between tremolite asbestos and talc. For example, the broad band around 532 cm^{-1}, which appears in the UV Raman spectra excited at both 257 and 244 nm, is absent in the spectrum of talc (Figure 3). This band has not been reported before in other studies on tremolite, in which Raman spectroscopic methods have been applied with excitation in the visible, near- and mid-IR regions.[6,12,25] Evident changes in the relative intensities of the Raman bands indicate chemical substitutions that often occur in asbestos minerals, particularly in the amphiboles. It is known that, for instance, Na and K often substitute for Ca (in tremolite and actinolite); also, Al and Ti can substitute for Si (Table 2). The most striking differences amongst the tremolite spectra excited with the 257- and 244-nm laser lines (Figure 3) occur in the lower wavenumber region of the coupled Si–O–Si deformation and metal–oxygen modes (below 450 cm^{-1}), where different patterns in the relative band intensities reflect the variability of the elemental composition. The mode at 1062 cm^{-1} is strongly enhanced in the spectrum of Figure 3a, and underlines the sensitivity and the high spatial resolution of UV Raman spectroscopy. The high signal-to-noise ratio of the UV Raman spectra of tremolite is supportively reflected in the results of the EDX analysis. The chemical composition of the tremolite sample used in this study was very close to the ideal composition (Table 4). The information obtained from UV Raman spectroscopy in combination with SEM/EDX analysis suggests that substitutions in the B sites of amphiboles seem to cause substantial structural rearrangements, whereas substitutions in the C and T sites are more easily tolerated.

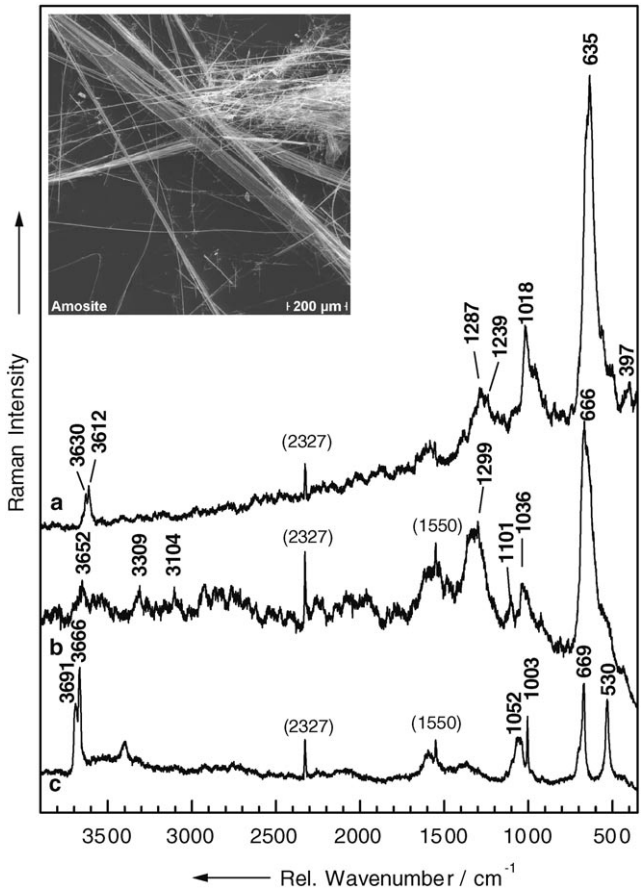

Figure 4. UV Raman spectra of amphibole asbestos: amosite (a), actinolite (b) and anthophyllite (c), each excited at 244 nm. The sharp signals at 2327 and 1550 cm^{-1} originate from N_2 and O_2 in ambient air, respectively. Inset: microphotograph of the asbestos mineral amosite.

2.4 Amphiboles: Anthophyllite, Actinolite, Amosite

Figure 4 shows the UV Raman spectra of amosite, actinolite and anthophyllite excited at 244 nm in the wavenumber range from 300 to 3900 cm^{-1}. The amphibole samples—except anthophyllite—showed low signal-to-noise ratios accompanied by sharp bands at 2327 (N_2) and 1550 cm^{-1} (O_2) from the ambient air. Tentative assignments of the observed UV Raman bands are also given in Table 5. Typical spectral features appeared in anthophyllite at 669 cm^{-1} from the symmetrical Si–O–Si stretching mode and in the two bands from the OH stretching modes in the high wavenumber region. A broad band in the region of the nonbridging $Si–O^-$ and the antisymmetric Si–O–Si stretching modes was recorded at 1052 cm^{-1}, which was shifted by 10 cm^{-1} from the band reported by Bard et al. in anthophyllite.[6] Again the symmetrically shaped strong band at 530 cm^{-1} was observed in the anthophyllite spectrum, which was obtained before in the spectra of chrysotile and tremolite (Figs. 2 and 3). Based on the complementary analysis by SEM/EDX (see Table 5) we suggest a tentative assignment of this band, which was observed for the first time by Rinaudo et al.,[15] to vibrations that emerge from the substitution of Fe for Mg in the C site of the asbestos minerals, but further investigations may be needed to verify this assignment.

3. Summary

UV micro-Raman studies have been performed on fibrous asbestos standards originating from representative localities, and the chemical composition of the samples has been determined using a scanning electron microscope in combination with an energy-dispersive X-ray analyser. From the results obtained it can be concluded that UV micro-Raman spectroscopy is highly sensitive to the structural variability caused by the chemical substitutions that typically occur in asbestos minerals. The observed Raman bands are sufficiently different, thus presenting a molecular fingerprint that allows differentiation between various species from the serpentine and amphibole asbestos groups.

Clark and co-workers have carried out investigations on reference standards of chrysotile, crocidolite and amosite, with an energy-dispersive spectrometer attached to an analytical transmission electron microscope.[27] The fibrous asbestos samples were analysed at several locations along the length of each fibre to assess the within- and between-fibre variability. The

analysis of the elemental composition in amosite revealed that the between-fibre variation consistently exceeded the within-fibre variation. However, in chrysotile and crocidolite fibres investigated by TEM/EDX this relationship was generally reversed, that is, the within-fibre components exhibited a higher variability in elemental composition than the between-fibre components. To address the variability of asbestos fibres in elemental composition on a more general basis, the authors have thus recommended to electron microscopic laboratories that a sufficient number of reference standards should be analysed, which is necessary for compiling a range of acceptable values of the chemical composition. Furthermore, since the data obtained from TEM experiments may vary from day to day, the authors also advised that a daily routine check of asbestos standards should be performed prior to the investigation of unknown asbestos samples. This procedure, however, is time-consuming, intense in laboratory costs and will never fully remedy the described obstacles of reliable identification of asbestos fibres.

UV Raman spectroscopy is a rapid analytical method which is suitably sensitive for supplementing or even replacing the established technique of SEM/EDX for an unambiguous discrimination of fibrous asbestos minerals. A major advantage of deep-UV Raman spectroscopy is that no fluorescence interference exists when excitation is provided at wavelengths below about 250 nm, because a typical Raman spectral range of 4000 cm^{-1} occurs in less than 30 nm above the excitation wavelength at 250 nm and no known material fluoresces at wavelengths below 280 nm. This effect therefore provides complete spectral separation of Raman and fluorescence emission bands, and results in the high signal-to-noise measurements required for a rapid and unambiguous identification of asbestos fibres. Furthermore, the Raman cross-section itself is dependent on the excitation wavelength to the inverse fourth power, which results in a higher Raman intensity with shorter-wavelength laser excitation and leads to a reduction in the acquisition time needed to record Raman spectra with a good signal-to-noise ratio.

Deep-UV Raman spectroscopy might be also well-suited to providing a new tool for rapid investigation of lung tissue obtained from patients on a routine basis via bronchoscopic surgery. The size of the sampling spot for micro-Raman experiments is proportional to the wavelength of the laser beam, and therefore a better spatial resolution for Raman mapping experiments is achieved when the excitation laser has a shorter wavelength. Therefore, it should be possible to localize the small asbestos fibres present per gram of lung tissue and to discriminate reliably between the various groups of amphibole or serpentine asbestos. These perspectives may throw fresh light on the long-lasting debate on the origin of the lethal diseases caused by fibrous asbestos minerals.

Acknowledgments

We acknowledge the financial support of the research project FKZ 13N8369 within the framework "Biophotonik" provided by the Federal Ministry of Education and Research (BMBF), Germany. We wish to thank U. Baierl for initiating this interesting topic and Dr. D. Papst-Baierl for fruitful discussions on the medical and health-insurance-related aspects involved in this study.

Keywords: asbestos · electron microscopy · minerals · Raman spectroscopy · X-ray absorption spectroscopy

[1] F. J. Wicks, D. S. O'Hanley, *Rev. Mineral.* **1988**, *19*, 91 – 101.
[2] K. Yada, *Acta Crystallogr.* **1967**, *23*, 704 – 707.
[3] K. Yada, *Acta Crystallogr. A* **1971**, *27*, 659 – 664.
[4] K. Yada, *Can. Mineral.* **1979**, *17*, 679 – 691.
[5] D. R. Veblen, A. G. Wylie, *Rev. Mineral.* **1993**, *28*, 61 – 138.
[6] D. Bard, J. Yarwood, B. Tylee, *J. Raman Spectrosc.* **1997**, *28*, 803 – 809.
[7] A. C. Allison, J. S. Harington, D. V. Badami, *Adv. Pharmacol. Chemother.* **1975**, *12*, 291 – 402.
[8] L. Michaels, S. S. Chissick, *Asbestos: Properties, Applications, and Hazards*, 1st ed., Wiley, New York, **1979**.
[9] A. M. Langer, R. P. Nolan in *Physicochemical Properties of Minerals Relevant to Biological Activities: State of the Art. Proceedings of the 3rd International Workshop on In Vitro Testing of Mineral Dusts*, 1st ed. (Eds.: T. Beck, J. Bignon), Springer, Berlin, **1985**.
[10] M. E. Gunter, *J. Geol. Educ.* **1994**, *42*, 17 – 24.
[11] M. Mellini, *Am. Mineral.* **1982**, *67*, 587 – 598.
[12] I. R. Lewis, N. C. Chaffin, M. E. Gunter, P. R. Griffiths, *Spectrochim. Acta A* **1996**, *52*, 315 – 328.
[13] M. Ross, R. P. Nolan, *Spec. Pap. Geol. Soc. Am.* **2003**, *373*, 447 – 470.
[14] C. Rinaudo, D. Gastaldi, E. Belluso, *Can. Mineral.* **2003**, *41*, 883 – 890.
[15] C. Rinaudo, E. Belluso, D. Gastaldi, *Mineral. Mag.* **2004**, *68*, 455 – 465.
[16] B. E. Leake, *Am. Mineral.* **1978**, *63*, 1023 – 1052.
[17] V. C. Farmer, *The Infrared Spectra of Minerals* , 1st ed. (Ed.: V. C. Farmer), Mineral. Soc., London, **1974**.
[18] J. T. Kloprogge, R. L. Frost, L. Rintoul, *Phys. Chem. Chem. Phys.* **1999**, *1*, 2559 – 2564.
[19] M. K. Titulaer, J. C. van Miltenburg, J. B. H. Jansen, J. W. Geus, *Clays Clay Miner.* **1993**, *41*, 496 – 513.
[20] G. W. Brindley, C. Kao, J. L. Harrison, M. Lipsiscas, R. Raythatha, *Clays Clay Miner.* **1986**, *34*, 239 – 249.
[21] R. L. Frost, S. J. van der Gaast, *Clays Clay Miner.* **1997**, *32*, 471 – 484.
[22] A. L. Auzende, I. Daniel, B. Reynard, C. Lemaire, F. Guyot, *Phys. Chem. Miner.* **2004**, *31*, 269 – 277.
[23] M. Odziemkowski, J. A. Koziel, D. E. Irish, J. Pawliszyn, *Anal. Chem.* **2001**, *73*, 3131 – 3139.
[24] W. A. Deer, R. A. Howie, J. Zussman, *An Introduction to Rock-Forming Minerals*, 2nd ed., Longman Scientific and Technical, Wiley, New York, **1992**.
[25] J. J. Blaha, G. J. Rosasco, *Anal. Chem.* **1978**, *50*, 892 – 896.
[26] W. B. White, *Infrared and Raman Spectroscopy of Lunar and Terrestrial Minerals*, 1st ed. (Ed.: C. Karr, Jr.), Academic Press, New York, **1975**.
[27] N. E. Clark, D. K. Verma, J. A. Julian, *Ann. Occup. Hyg.* **1995**, *39*, 79 – 88.

Received: June 3, 2005
Published online on January 3, 2006

